BASIC RESEARCH PAPER

Autophagy 11:7, 1099–1113; July 2015; Published with license by Taylor & Francis

Single-cell analysis challenges the connection between autophagy and senescence induced by DNA damage

Eduardo Cremonese Filippi-Chiela,[1] Mardja Manssur Bueno e Silva,[1] Marcos Paulo Thomé,[1] and Guido Lenz[1,2,*]

[1]Department of Biophysics; Federal University of Rio Grande do Sul (UFRGS); Porto Alegre, Rio Grande do Sul, Brazil; [2]Center of Biotechnology; Federal University of Rio Grande do Sul (UFRGS); Porto Alegre, Rio Grande do Sul, Brazil

Keywords: autophagy, DNA damage, senescence, single cell, temozolomide

Abbreviations: 3MA, 3-methyladenine; AO, acridine orange; BafA1, bafilomycin A_1; CDKN1A/p21, cyclin-dependent kinase inhibitor 1A (p21, Cip1); cP1-4, cellular population 1 to 4; CPD, cumulative population doubling; DDR, DNA damage response; DFM, drug-free medium; H2AFX, H2A histone family, member X; MAP1LC3A/LC3, microtubule-associated protein 1 light chain 3 α; MTOR, mechanistic target of rapamycin; MTORC1, MTOR complex 1; NA, nuclear area; NMA, nuclear morphometric analysis; nP1–5, nuclear population 1 to 5; PRKAA/AMPKα, protein kinase, AMP-activated; RAPA, rapamycin; RPTOR/RAPTOR, regulatory-associated protein of MTOR, complex 1; SA-β-gal, senescence associated β-galactosidase assay; SQSTM1/p62, sequestosome 1; TMZ, temozolomide.

Autophagy and senescence have been described as central features of cell biology, but the interplay between these mechanisms remains obscure. Using a therapeutically relevant model of DNA damage-induced senescence in human glioma cells, we demonstrated that acute treatment with temozolomide induces DNA damage, a transitory activation of PRKAA/AMPK-ULK1 and MAPK14/p38 and the sustained inhibition of AKT-MTOR. This produced a transient induction of autophagy, which was followed by senescence. However, at the single cell level, this coordinated transition was not observed, and autophagy and senescence were triggered in a very heterogeneous manner. Indeed, at a population level, autophagy was highly negatively correlated with senescence markers, while in single cells this correlation did not exist. The inhibition of autophagy triggered apoptosis and decreased senescence, while its activation increased temozolomide-induced senescence, showing that DNA damage-induced autophagy acts by suppressing apoptosis.

Introduction

Macroautophagy (hereafter referred to as autophagy) is a physiological catabolic process that is involved in maintaining the quality of cellular components and energetic homeostasis. Autophagy is directly coordinated by the *ATG* genes and indirectly modulated by several signaling pathways involved in cell metabolism and growth, such as the positive regulators PRKAA/AMPK and nuclear TP53 (TRP53 in mice) and the negative regulators PI3K-AKT and the MAPK pathways. These pathways have, as a common target in autophagy, the MTOR (mechanistic target of rapamycin) protein, which directly controls the initial autophagy steps.[1,2]

Autophagy is involved in several processes, such as aging and cancer.[3] It appears to contribute to controlling the life span of several species, ranging from plants[4] to mammals;[5] this is corroborated by the observation that several longevity pathways, such as IGF1 (insulin-like growth factor 1 [somatomedin C]), sirtuins and FOXO, modulate autophagy.[6-8] In cancer, autophagy is thought to act as a tumor suppressor mechanism during tumor initiation by contributing to the maintenance of genomic integrity and the elimination of procarcinogens.[9-11] Accordingly, genetic alterations on autophagic genes, such as *BECN1* and *ATG7*, have been associated with a higher tumor incidence and resistance to therapies;[9,12,13] several tumor suppressor genes also induce autophagy, such as *PTEN*, *TSC1*/*2,* and *STK11*/*LKB1*.[14] However, in established solid tumors, autophagy may contribute to tumor adaptation and survival during metabolic stress in addition to favoring cell resistance to therapy.[15] Autophagy is triggered by several therapeutic interventions, including those that induce the DNA damage response (DDR).[16] Autophagy also interferes with the fate of cancer cells in 2 ways: by favoring cell

*Correspondence to: Guido Lenz; Email: lenz@ufrgs.br
Submitted: 04/23/2014; Revised: 07/18/2014; Accepted: 12/10/2014
http://dx.doi.org/10.1080/15548627.2015.1009795

survival or by contributing to cell death.[17] Increasingly, it has been shown that autophagy exerts its effects through the modulation of apoptosis, the cell cycle, and senescence.[18,19] Autophagy normally blocks apoptosis,[20] but the role of autophagy in senescence remains unclear, though these mechanisms are known to play a central role in aging and carcinogenesis.[21,22]

Senescence is a state of irreversible cell growth arrest and metabolic activity maintenance. It acts as an endogenous antitumor mechanism by avoiding the proliferation of transformed, pretumor cells.[23-25] However, it has been associated with tumor resistance in apoptosis-resistant cancer cells because senescent cells remain metabolically active and can affect the growth of surrounding cells through paracrine signaling.[26-28] Senescence can be triggered by cell aging, oncogenic activation or in response to drugs that affect DNA and mitochondria, among other cell components.[23,29] Senescence establishment is driven by proteins that control the cell cycle and the stress response, such as the TP53, CDKN1A/p21, CDKN1B/p27, and CDKN2A/INK4/ARF proteins.[23,29, 30]

The studies that addressed the role of autophagy on senescence "did not present an overview of the temporal induction of autophagy and senescence," as recently stated.[21] To shed light on this issue, we used a model of DNA damage-induced autophagy and senescence by treating glioma cells with the alkylating agent temozolomide (TMZ), which is the main chemotherapeutic agent used in gliomas.[31-33] We found that acute DNA damage triggered a transient autophagy, followed by senescence induction. Although autophagy and senescence are strongly correlated at a population level, no direct interdependence was observed in individual cells. Additionally, the inhibition of autophagy triggered apoptosis and reduced senescence.

Results

Acute treatment with TMZ induced long-term senescence

U87 glioma cells stably expressing the autophagy marker GFP-LC3 (GFP fused to MAP1LC3A, microtubule-associated protein 1 light chain 3 α) were treated with 100 μM TMZ for 3 h, followed by replating the cells in drug-free medium (DFM) (**Fig. 1A**). The phosphorylated form of H2AFX at Ser139 (commonly termed γ-H2AFX), an indicator of DDR activation, was transiently increased with a peak at day 3 (D3); this was accompanied by a gradual increase in the phosphorylated form of CDC2 (Tyr15), which inhibits the activity of the CCNB1-CDK1 complex at G_2/M, and an induction of the CDK inhibitor CDKN1A/p21. This signaling is indicative of the activation of the G_2/M checkpoint, which is corroborated by the decrease of both HIST1H3A/C histone Ser10 phosphorylation and the CCND1 (cyclin D1) levels (**Fig. 1B**). As expected, TMZ produced an accumulation of cells at G_2/M, peaking on D3; this was followed by a gradual increase in the hyperdiploid and multinucleated cells (**Fig. 1C**). The cumulative population doubling (CPD) indicated that the acute TMZ treatment led to a stabilization of the cell number, suggesting permanent cell growth arrest (**Fig. 1D**). The CPD profile suggested the beginning of senescence, which was corroborated by an increase in the percentage of cells positively marked with the senescence-associated β-galactosidase (SA-β-Gal$^+$ cells) (**Fig. 1 E**) and an increase in the percentage of cells with large and regular nuclei, a morphological feature of senescent cells (**Fig. S1A**); as observed through the nuclear morphometric analysis (NMA) technique.[34] Interestingly, when NMA was analyzed as a contour plot, it was possible to observe a dynamic distribution of the nuclei over time in 3 well-defined regions, as described in the legend of **Fig. 1**. The nuclear area (NA) from the TMZ-treated cells progressed from NA1 to NA3, which is characteristic of senescent cells, through the intermediary state, NA2. On D7, only a few cells remained that had a nuclear area of nonsenescent cells (NA1) or that were in the intermediary region NA2 (**Fig. 1F** and **Fig. S1B**).

Acute TMZ treatment triggers early PRKAA/AMPK-ULK1 and MAPK14/p38 activation, persistent AKT-PI3K-MTOR suppression and transient autophagy

The acute TMZ treatment induced an increase in p-PRKAA/AMPKa (Thr172) on D3, accompanied by an increase of 2 PRKAA targets:[35] p-ULK1 (Ser555), a member of the initial complex of autophagy promotion (ULK1-RB1CC1/FIP200-ATG13), and p-RPTOR (Ser792), which disrupts the formation of the complex 1 of MTOR (MTORC1) when phosphorylated, leading to autophagy induction.[36] Accordingly, MTOR activity, as indicated by p-RPS6KB1/p70S6K1 (Ser389), p-MTOR (Ser2448), p-EIF4EBP1/EIF4EPB1 (Thr37/46), p-AKT (Ser473) and p-GSK3B (Ser9), was gradually reduced, remaining low on D7. MAPK14/p38, an important sensor of cell damage (including genomic injury), had increased levels of phosphorylation on D3 and D5 (**Fig. 2A**). It is important to note that the phosphorylation of MAPK14, PRKAA, and ULK1 follows kinetics that resemble the primary DNA damage that was produced (**Fig. 1B**), whereas the remaining proteins had slower and longer lasting post-translational modifications. These data are supportive of proautophagic signaling after DNA damage, involving the activation of the PRKAA-ULK1 axis and the suppression of the AKT-MTORC1 pathway.

Indeed, TMZ led to an increase in the proportion of GFP-LC3$^+$ cells (**Fig. 2B**). The proportion of acridine orange (AO)-positive cells increased until D4, followed by a sudden increase in the mean level of AO staining with a concomitant reduction in the proportion of AO+ cells (**Fig. 2C**, **Fig. S1C** and **D**). Autophagy induction was also confirmed by western blot for the LC3-I to LC3-II conversion and the levels of the SQSTM1/p62 protein, which is degraded during autophagy (**Fig. 2D**). These data confirm that acute DNA damage triggers autophagy, peaking on approximately D3 and D4 followed by a gradual reduction. Despite the high levels of autophagy, a reduction of the intracellular ATP levels was observed after the TMZ treatment (**Fig. 2E**).

The connection between autophagy and senescence is highly heterogeneous at the individual cell level

When 2 well-defined mechanisms are induced in a population of heterogeneous cells, it begs the question whether what is

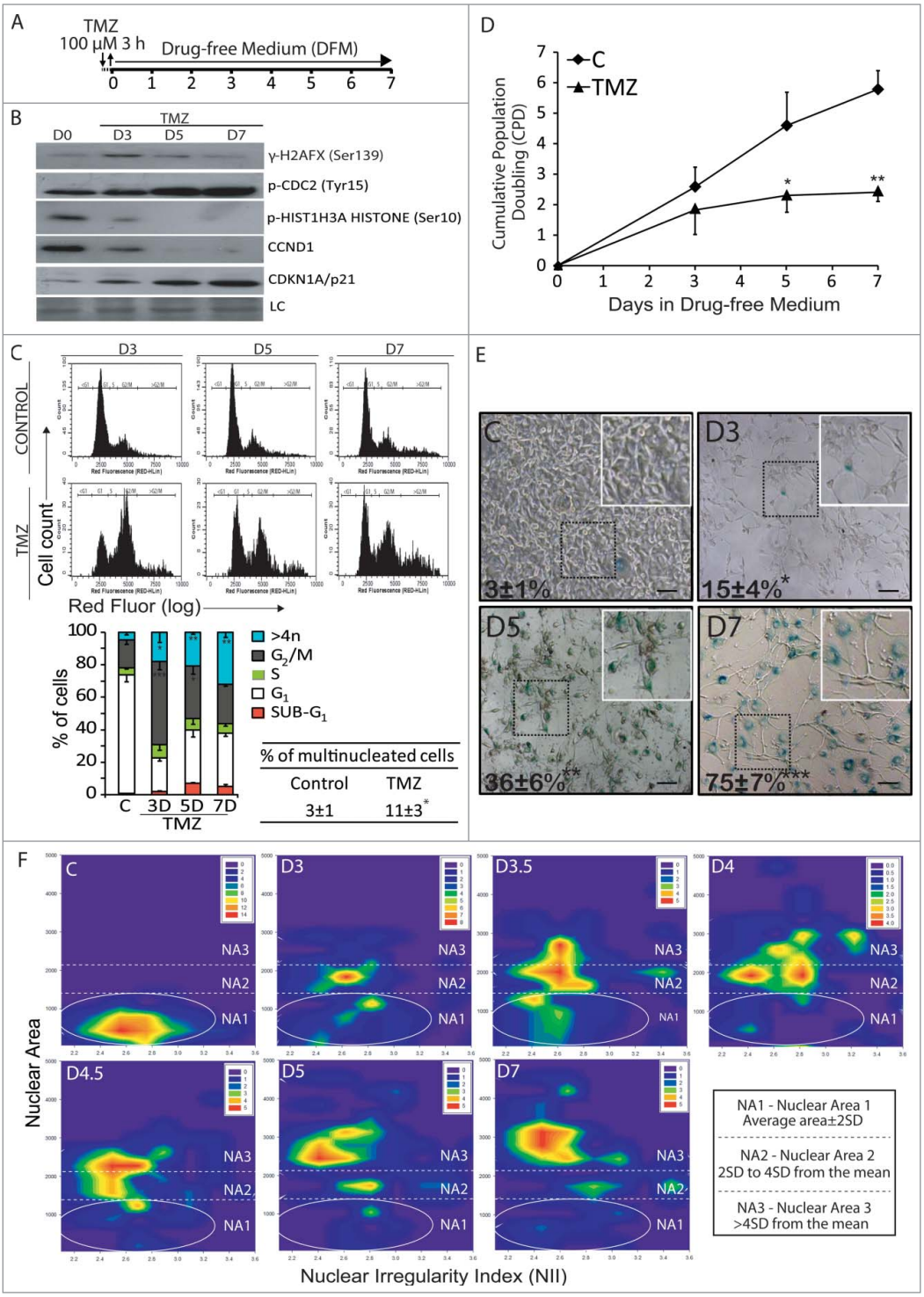

Figure 1. Acute treatment with TMZ induces cell cycle arrest and senescence in glioma cells. (**A**) The U87 cells stably expressing GFP-LC3 were treated with 100 μM TMZ for 3 h, followed by growth in the drug-free medium (DFM) for the indicated time. Time zero (D0) represents 3 h after treatment. (**B**) The Western blot for the indicated proteins on D3, D5, and D7 after DFM replating; LC, loading control, *Coomassie blue* stained membrane. (**C**) The cell cycle distribution. *Top*, representative plots; *bottom left*, quantification of the percentage of sub-G_1, G_1, S, G_2/M and hyperdiploid cells; *bottom right*, percentage of multinucleated cells, assessed by the direct counting of cells with 2 or more nuclei with a normal area on D7. (**D**) Cumulative population doubling (CPD) of the cells treated as in (**A**). (**E**) Representative images of the SA-β-gal staining; the numbers represent the quantification of the percentage of β-gal-positive cells (mean ± SEM); scale bar = 80 μm. (**F**) The NMA contour plot of the TMZ-treated cells over time. The nuclear areas (NA) were defined based on the average of the normal nuclei, and the thresholds were determined by the mean area ± 2 SD (NA1), 2 SD to 4 SD from the mean (NA2) and more than 4 SD from the mean (NA3). NII represents the index of nuclear irregularity, as a measurement of nuclear morphometric alterations that occur over time. The values on the heat map legends represent the number of cells. $^*P < 0.05$; $^{**}P < 0.01$, $^{***}P < 0.001$ in relation to the control.

observed for a population is an average of a heterogeneous response or the depiction of a homogeneous effect. An analysis of the GFP-LC3 area in relation to the nuclear area showed a population transition from an initial state with neither autophagy nor senescence markers (nuclear population 1 - nP1), passing through a state of high autophagy (nP2 and nP3) and a nuclear area in the NA2 region, and finally reaching a state of low autophagy and intermediary (nP4) or large (nP5) nuclei on D7 (**Fig. 3A**). Similar dynamics were observed for the area of the cell, except for a delay of 1 to 2 d that was required for the cell area to pass from an intermediary region (cP3) to the region corresponding to the state of the largest cell area (cP4) (**Fig. 3A**).

When the proportion of cells with a given phenotype is analyzed, a critical period can be observed between D3 and D4.5 in which autophagy reaches its maximum levels accompanied by the beginning of senescence; this can be observed from the CPD and β-Gal staining (**Fig. 3B**). To evaluate how individual cells go through this transition, we measured autophagy and senescence

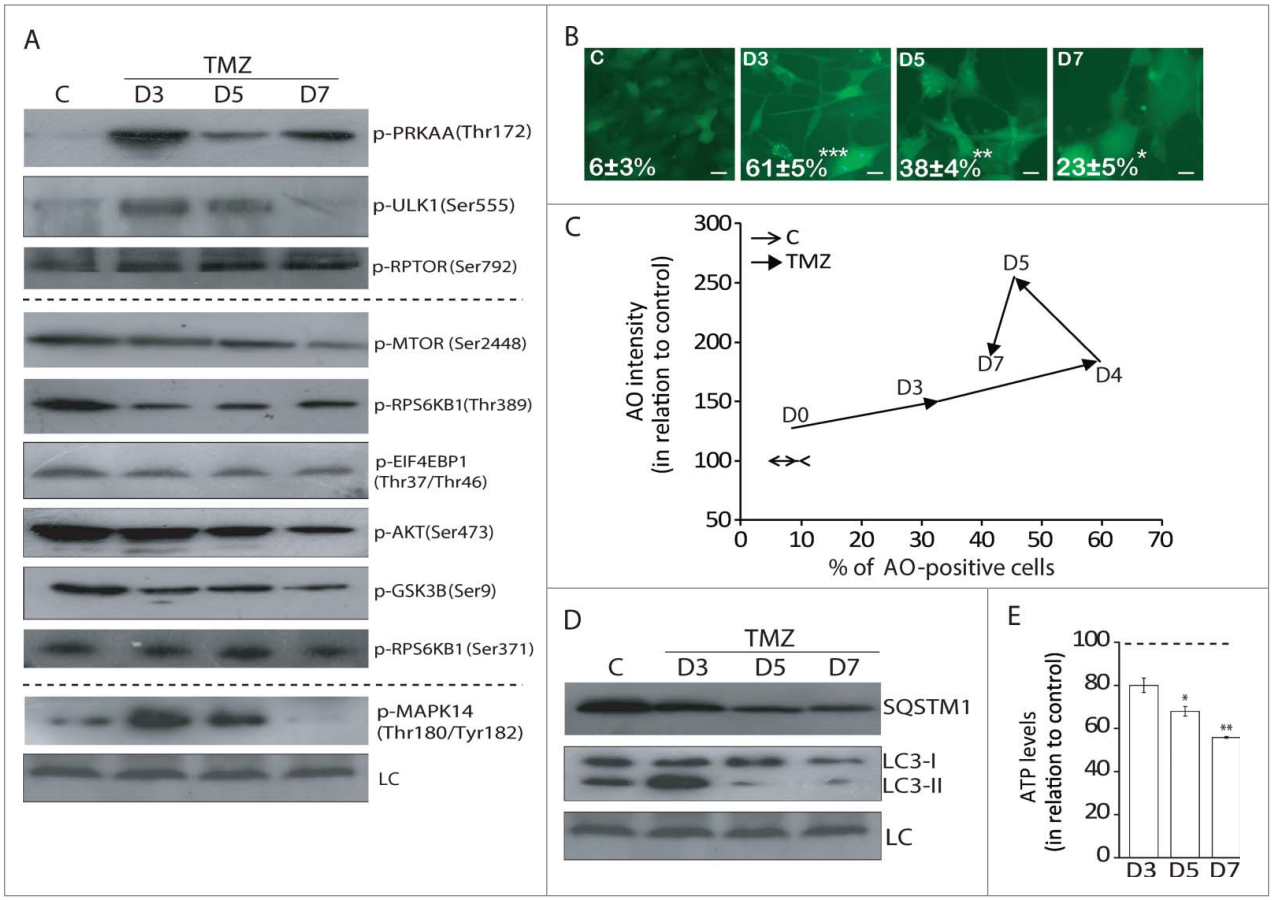

Figure 2. Acute treatment with TMZ induces autophagy accompanied by early AMPK-ULK1 axis activation and long lasting AKT-PI3K-MTOR suppression. (**A**) The U87 cells were treated as described in **Figure 1A**, and western blots for the indicated proteins and phosphoproteins were performed; LC, loading control, *comassie blue* stained membrane. (**B**) The GFP-LC3 dot formation assay; the numbers depict the percentage of cells with at least 5 GFP-LC3 dots (mean ± SEM); $^{*}P < 0.05$, $^{**}P < 0.01$ and $^{***}P < 0.001$; scale bar = 20 μm. (**C**) Acridine orange (AO) staining: the graph shows the percentage of AO-positive cells *versus* the AO intensity of the positive population in relation to the control over time (to see the data of AO intensity and the percentage of cells in a separate manner, see **Fig. S1C** and **S1D**). (**D**) Western blots for SQSTM1 and LC3-I/LC3-II. LC, loading control, *comassie blue* stained membrane. (**E**) The ATP levels of the cells treated with TMZ as in **Figure 1A**; $^{*}P < 0.05$ and $^{**}P < 0.01$ in relation to the control, which was considered 100%.

markers by tracking individual cells from D3 to D4.5. In the control cells, LC3, the cell and nuclear areas remained virtually constant (see examples in **Fig. 4C**). However, the TMZ-treated cells underwent a very heterogeneous response, which can be observed in the path shown in a cell area versus GFP-LC3 area graph (**Fig. 3C**). We found some cells that had very similar positions in the LC3 vs. cell area graph on D3 but reached very different positions by D4.5 (**Fig. 3C**); some cells passed through a position in the graph with similar GFP-LC3 and cell areas but were coming from and going to very different positions in this graph (**Fig. 3C**); and some cells reached a similar position even though they started at different points and went along very different paths (**Fig. 3C**). A similar heterogeneous response was observed for the nuclear area (**Fig. S2A–D**).

To try to make sense of this very heterogeneous response, we plotted the vectors of all the cells over the intervals of the analysis in relation to the initial value (considered as 1). The high degree of heterogeneity concerning the nuclear and cell areas in relation to GFP-LC3 became evident during the intervals from D3 to D3.5 and D3.5 to D4 (**Fig. 3D**, left and middle graphs). However, from D4 to D4.5, a clear reduction in the level of autophagy occurred in more than 90% of the cells, resulting in a very low GFP-LC3 area (**Fig. 3D**, right graph). Importantly, the non-normalized data indicated that this reduction in GFP-LC3 occurred independently of the cell and nuclear areas (**Fig. S2E**), suggesting an orchestrated mechanism of autophagy that ended after the DNA damage, independent of the area of the cell or nucleus and, likely, of the process of senescence induction. As expected, 85% of the control cells did not trigger autophagy; there was no significant increase in the cell area or the nuclear area (**Fig. S2F**).

Population vs. single cells analysis of autophagy and senescence

Despite this heterogeneous response in individual cells, at a population level, a significantly larger nuclear area was observed in the few cells that were already βgal-+ on D3 in relation to the

βgal$^-$ cells. Interestingly, the GFP-LC3 status was inversely correlated with the nuclear area in the βgal$^+$ cells but not in the βgal$^-$ cells, with the LC3$^-$ cells being significantly larger than the LC3$^+$ cells in the former (**Fig. 4A**). This was also observed after treatment with another DNA damaging agent, Doxorubicin, at a concentration of 100 nM for 24 h followed by 7 d in DFM (**Fig. S3A**). This effect, along with the reduction in autophagy that was observed in the majority of the cells, raised the question of whether autophagy reduction precedes senescence entry.[21,37] To answer this, we measured the interval in which the GFP-LC3 area undergoes the largest alteration for each cell, and, in parallel, the interval in which each cell undergoes the largest increase in area between D3 and D4.5. Roughly one-third of the cases fell into each of the 3 possibilities, i.e., autophagy reduction before, concomitant with or after the largest increase in cell area (**Fig. 4B**). As mentioned above, the control cells barely altered their phenotype over time (**Fig. 4C**).

After D7 in DFM, the distribution of the LC3$^+$ and LC3$^-$ cells was more uniform in the βgal$^-$ cells compared to the βgal$^+$ cells, suggesting that the progression to senescence eventually includes the reduction of LC3, which is less likely to occur in cells that also received the initial proautophagic damage but did not progress toward senescence (**Fig. 5A, B** and **Fig. S3B**). Of the cells that were still LC3$^+$ on D7, approximately 66% had a normal nuclear area (NA1), and the proportion of LC3$^+$ cells gradually decreased from the NA1 to NA3 population (**Fig. 5A**, black bars on the right).

Altogether, this indicates that when analyzed at a population level, autophagy markers increased

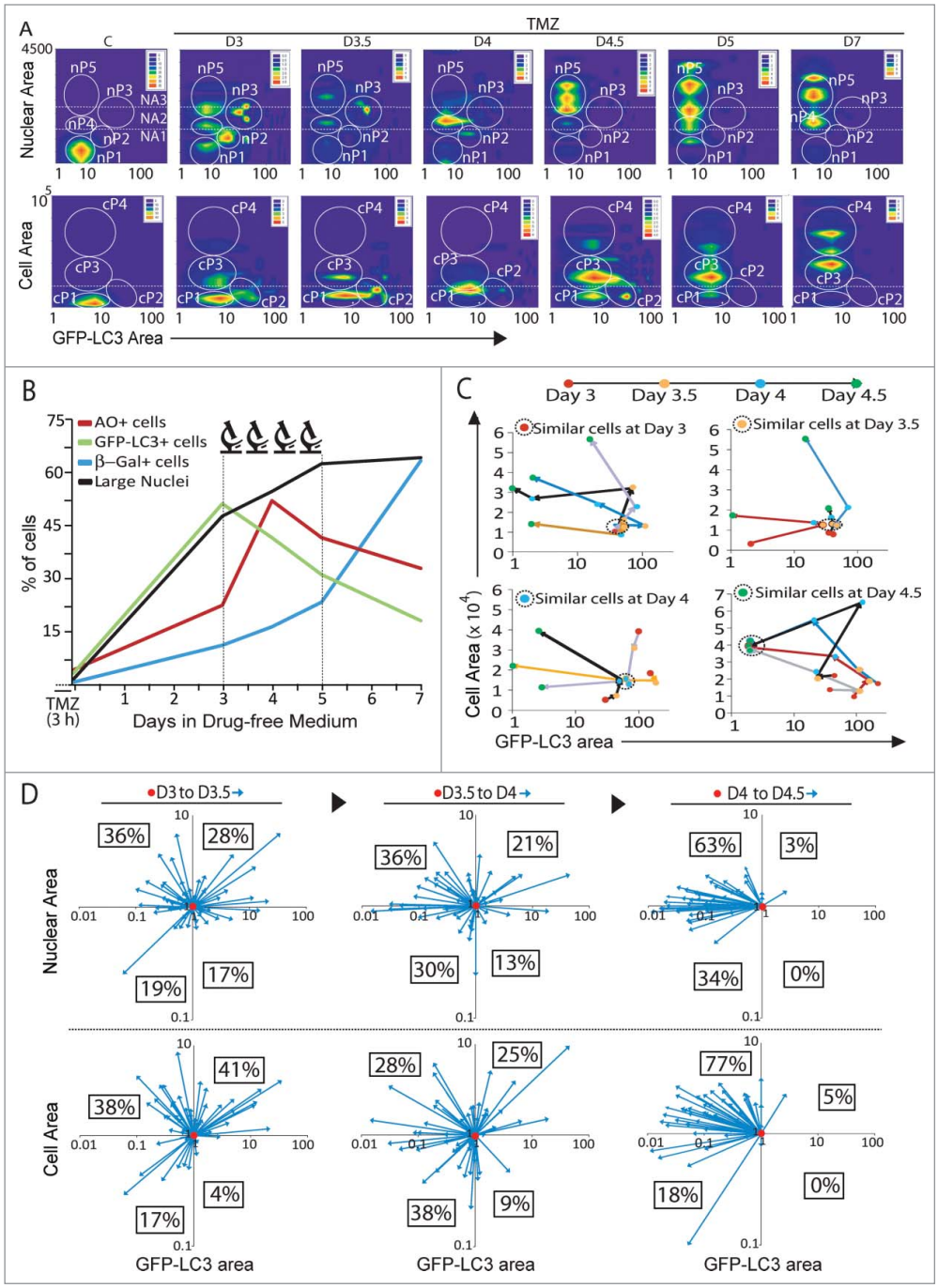

Figure 3. The single-cell analysis of the GFP-LC3, nuclear, and cell areas after TMZ treatment. (**A**) Contour plots of the cell and nuclear areas in relation to the GFP-LC3 area after treatment as described in **Figure 1A**. The circles mark the populations based on regions with high density that emerged from the plots of nuclear area (nP, *top*) and cell area (cP, *bottom*) in relation to GFP-LC3; the dashed lines mark the thresholds of NA1, NA2, and NA3, as indicated in **Figure 1F**. The values on the heat-map legends represent the number of cells for each color. (**B**) Summary of autophagy and the senescence marker after TMZ treatment. The single cells were photographed every 12 h from D3 to D4.5. (**C**) Single cell tracks for groups of cells that presented similar GFP-LC3 and cell area on D3 (first graph), 3.5 (second graph), 4 (third graph) and 4.5 (fourth graph), based on the cell area and the GFP-LC3 area. Each colored line in each graph represents a single cell track. The days of analysis are coded by colored circles (red: Day 3; orange: D 3.5; blue: D 4; green: D 4.5). The cells with similar characteristics in each day are surrounded by an ellipse with a dotted line. (**D**) The vectors of the GFP-LC3 area versus the nuclear (top) or cell (bottom) areas, considering the initial value as 1 for each interval (red circle); the numbers represent the percentage of cells in each quadrant at the end of the interval.

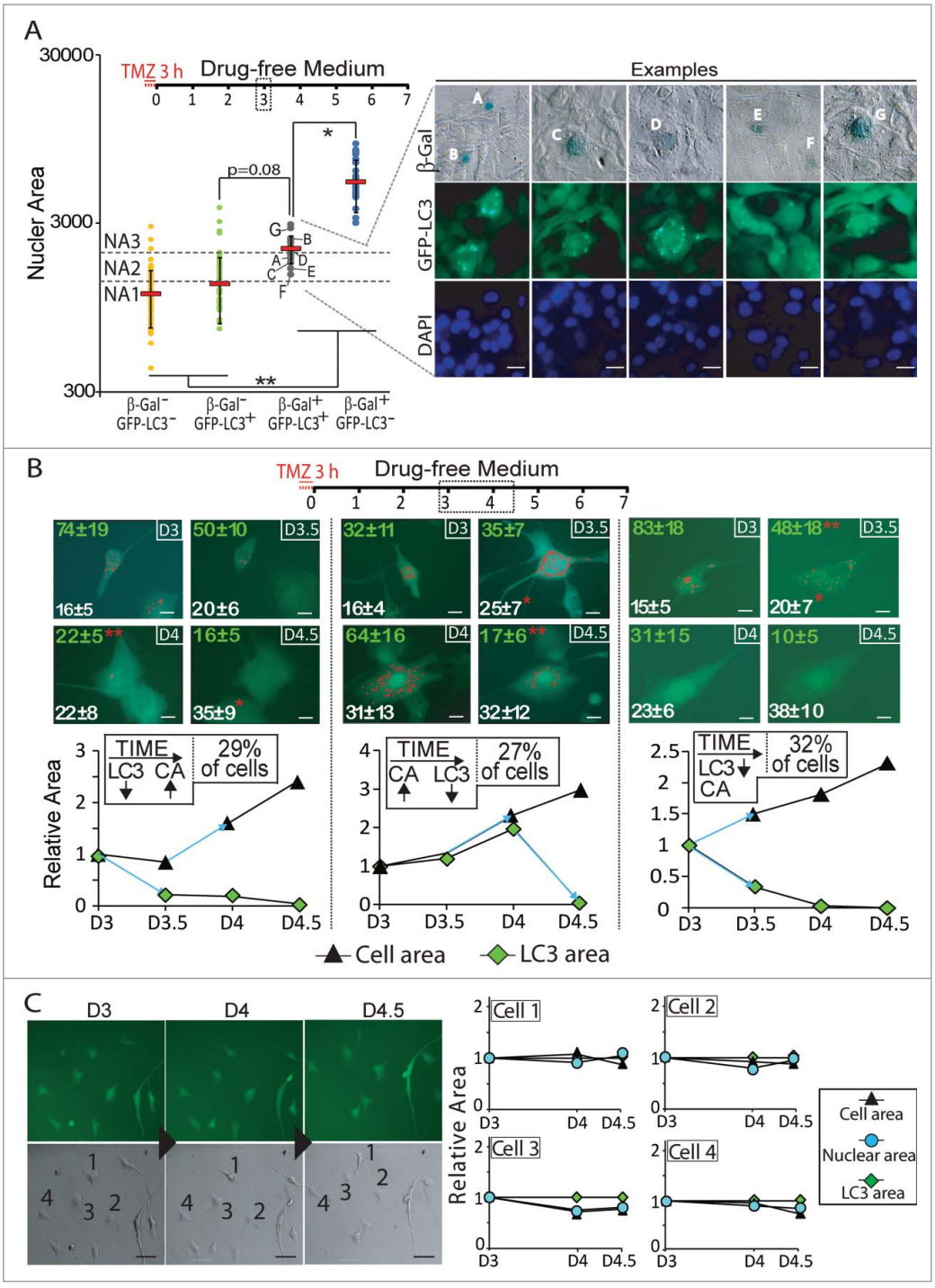

Figure 4. Autophagy decreases after, before, or concomitant to the acquisition of the senescent phenotype in single cells. (**A**) LC3 and SA-β-gal staining in relation to the nuclear area on D3 (*left*-); in red, average ± SEM; **P* < 0.05 and ***P* < 0.01. The letters in the graph (A to G) correspond to the representative examples of the SA-β-gal and LC3 double-positive cells shown on the *right*; scale bar = 20 μm. The number of events shown does not represent the ratio of each population of cells. (**B**) GFP-LC3 reduction before (*left*), after (*mid*) or concomitant with (*right*) cell enlargement. *Top*, the red dots in the GFP-LC3 images correspond to the GFP-LC3 dots as they were marked in the Image Pro Plus software. The numbers in the images represent the mean ± SEM of the GFP-LC3 area (green) and the cell area $\times 10^3$ (white). Statistics represent the first significant reduction of GFP-LC3 area and increase of cell area in comparison to the areas in the previous time point (**P* < 0.05 and ***P* < 0.01). Scale bar = 20 μm. *Bottom* –representative GFP-LC3 (LC3) and cell area (CA) profiles of single cells of the 3 groups. To define these profiles, we measure the intervals in which each cell underwent the highest alteration in LC3 and cell areas. These intervals are shown in the representative graphs as blue arrows. The data are shown in relation to the D3 value, considered as 1. The inserts in the boxes denote the percentage of cells in each profile. (**C**) Representative images (left) and graphs (right) of the control cells assessed at the single cell level on d 3 to 4.5. The data are shown in relation to the control, which was considered as 1 on D3.

with faster and transient kinetics (**Fig. 2B–D**; **Fig. 3B**), while senescence markers increased with slower and sustained kinetics (**Fig. 1A, C, D** and **F**; **Fig. 3B**). Autophagy decreased before senescence became dominant in the population, which was observed through the inverse correlation between the variation of the cell or nuclear areas and the variation of the LC3 area from D3 to D4.5 in the population. This inverse correlation was also high when considering data from D3 to D7 (**Fig. 5D**, bottom line; **Fig. S3C**). However, for individual cells, we found a highly heterogeneous response regarding the correlation between the variation of the LC3 area and the variation of the cell area (**Fig. 5C**, first column) or the nuclear area (**Fig. 5C**, middle column). As a consequence, the average of the single cell correlation values did not indicate a positive or negative correlation (**Fig. 5D**, right). These data corroborate the high heterogeneity of the response observed at the single cell level during the critical period from the high autophagy and low phenotypic features of senescence (D 3) to the condition of low autophagy with the appearance of

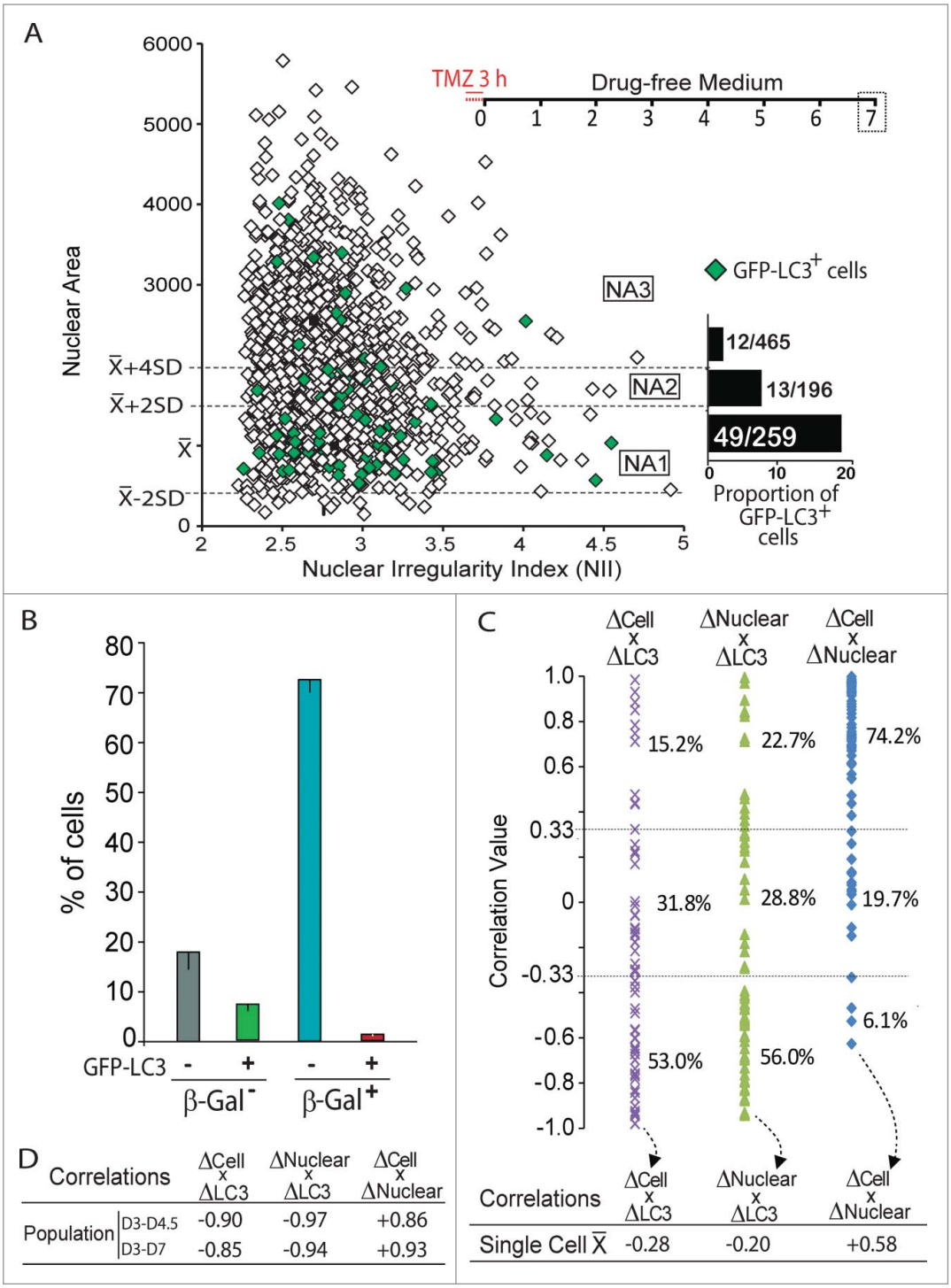

Figure 5. The autophagy and senescence markers are highly correlated at the population level but not at the individual cell level. (**A**) The distribution of the GFP-LC3$^+$ cells according to the nuclear area on D7. The red circle marks the normal nuclear area. NA1, NA2, and NA3 are shown as the dashed lines. On the right is shown the proportion of the GFP-LC3$^+$ cells in relation to the total cells in each nuclear area (NA) region. (**B**) Profile of the GFP-LC3 and SA-β-gal staining (positive and negative) on D7. (**C**) Correlations between the variations of the cell and nuclear areas and the total LC3 area for all single cells from D3 to D4.5. (**F**) Bottom: average of the correlations for the single cells and the correlations of the average of the population of cells from D3 to D4.5 and from D3 to D7.

senescence markers (D 5 onwards). Thus, our data show that the reduction in autophagy does not have to precede an increase in the cell or nuclear areas in a single cell, and that the acquisition of senescent phenotype is not necessary for autophagy reduction, though this was the predominant event in the population.

Inhibition of TMZ-induced autophagy triggers apoptosis and reduces senescence

The inhibition of autophagy with bafilomycin A_1 (BafA1) on D3 for 24 h reduced the TMZ-induced autophagy only during its presence (i.e., from D3 to D4), followed by a rebound in both the percentage and intensity of the AO staining to levels even higher than those induced by the TMZ alone (**Fig. 6A**, left; **Fig. S4A, B**). This effect may be due to the accumulation of autophagosomes because BafA1 suppresses the fusion between autophagosomes and lysosomes through the blockage of lysosome acidification.[38] However, 3-methyladenine (3MA) reduced the AO staining (**Fig. 6A**, right; **Fig. S5A, B**) in addition to reducing GFP-LC3 dot formation (**Fig. 6B**). Furthermore, the autophagy inhibition with 3MA induced apoptosis, which was indicated by cell shrinkage (**Fig. 6B** and **Fig. S4C**), CASP3/caspase 3 cleavage (**Fig. 6C**) and an increase in small and regular nuclei (**Fig. 6D**), a typical feature of apoptotic cells.[34] Interestingly, though it also reduced autophagy, the BafA1 treatment did not lead to apoptosis.

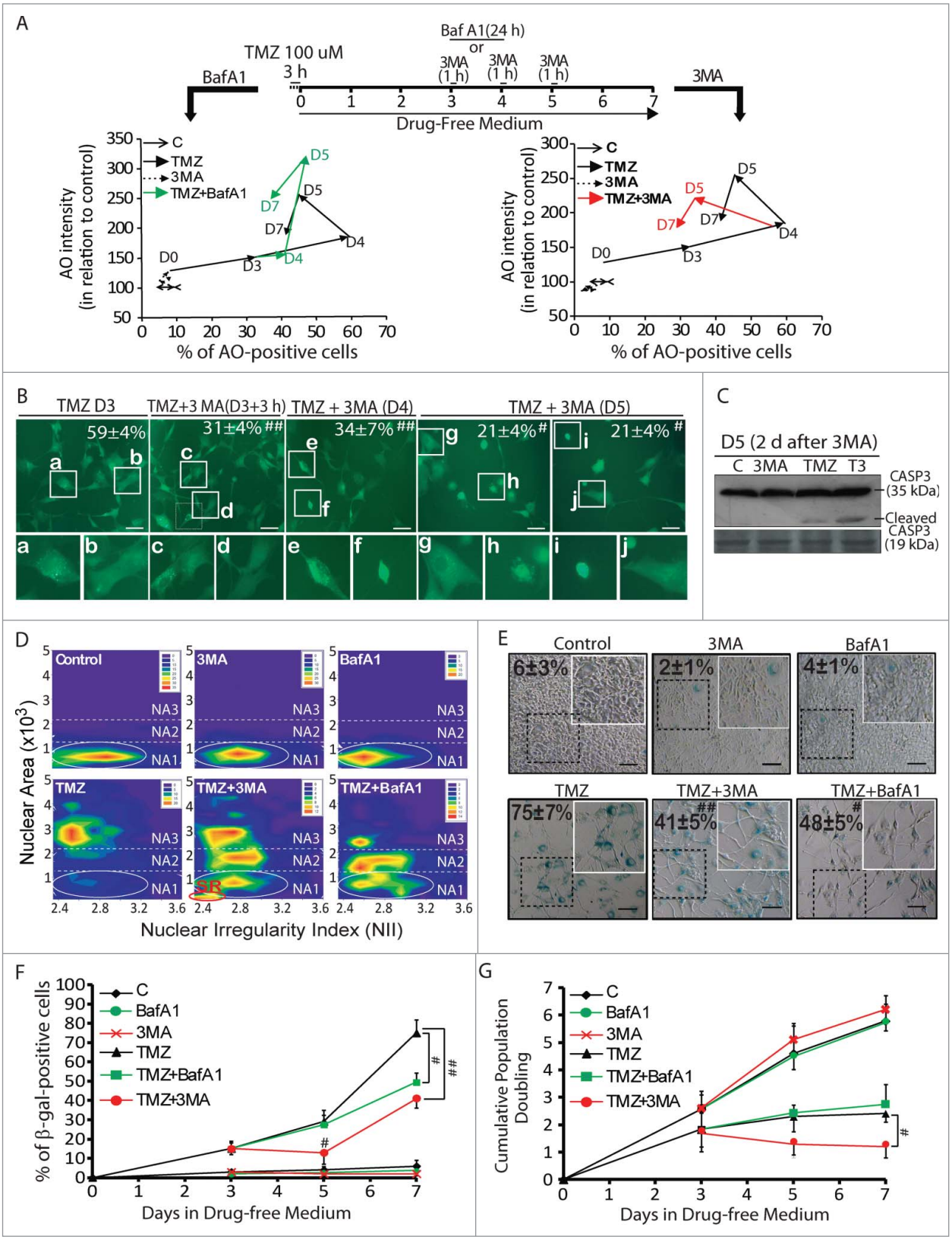

Figure 6. For figure legend, see page 1107.

On D3, some nuclei of the TMZ-treated cells were already in the NA2 and NA3 regions, but by D7, almost all the nuclei were in the NA3 population (**Fig. 1D**). The inhibition of autophagy with either BafA1 or 3MA kept the nuclei in the NA1 and NA2 populations (**Fig. 6D**), in agreement with the reduction in the proportion of βGal^+ cells (**Fig. 6E and F**). Finally, the treatment with 3MA reduced the number of cells from D3 onwards, likely due to the induction of apoptosis, which was not observed after the BafA1 treatment (**Fig. 6G**).

Rapamycin increased TMZ-induced senescence

Treatment with the MTOR inhibitor rapamycin (RAPA) on D5 (**Fig. 7A**) led to a large increase in GFP-LC3 dot formation (**Fig. 7B**) and AO staining (**Fig. 7C** and **Fig. S5A, B**) in comparison to the TMZ treatment alone. This acute increment of autophagy from D5 to D6 led to an increase in the percentage of βgal^+ cells on D7 in comparison to TMZ alone (**Fig. 7D**) and a reduction in the number of cells (**Fig. 7E**). Furthermore, while we observed some mitotic figures on D7 in the TMZ-treated cells, we did not observe these phenotypes in the TMZ+RAPA-treated cells (**Fig. 7E**, insert).

Accordingly, the RAPA treatment 24 h before the TMZ treatment (**Fig. 7F**) anticipated the peak of the TMZ-induced autophagy, which was measured with GFP-LC3 (**Fig. 7G** and **Fig. S5C**) and AO (**Fig. 7H** and **Fig. S5D, E**). The RAPA pretreatment accelerated the TMZ-induced senescence entry, as shown by the βgal staining (**Fig. 7I**), the CPD analysis and the CDKN1A levels (**Fig. 7J**). It is interesting to note that RAPA alone, despite inducing a higher initial proautophagic effect than TMZ (**Fig. 7G, H** and **Fig. S5C–E**), did not induce a sustained autophagy or senescence response.

Inhibiting and activating autophagy at different times as a form of increasing the efficacy of TMZ

The cells with nuclei in the NA2 region on D3 (**Fig. 1F**) responded differently according to their autophagic status: high LC3 cells increased their average nuclear area from D3 to D4.5, whereas low LC3 cells maintained the same area or decreased their nuclear area, i.e., underwent apoptosis (**Fig. 8A**). Therefore, we wondered whether activating and blocking autophagy at different times could potentiate the effects of TMZ by increasing senescence and inducing apoptosis. Indeed, the RAPA pretreatment followed by the TMZ treatment and the addition of 3MA on D3, D4, and D5 led to a further reduction in the number of cells in comparison to the treatments individually (**Fig. 8B**).

Discussion

In this study we found that (i) acute DNA damage leads to PRKAA/AMPK-ULK1 and MAPK14 activation and sustained downregulation of the AKT-PI3K-MTOR pathway, leading to a transient activation of autophagy (**Fig. 8C**); (ii) at a population level, autophagy is highly negatively correlated with senescence markers, while in single cells this correlation does not exist (**Fig. 4F**); and (iii) boosting senescence by inhibiting MTOR prior to DNA damage, together with later inducing apoptosis by inhibiting autophagy, may be a good strategy to reduce the number of cancer cells.

The dynamics of autophagy induction resembled the kinetics of DDR and the activation of the PRKAA/AMPK-ULK1 and MAPK14/p38 pathways, while the orchestrated reduction of autophagy on D4 occurred despite the sustained MTOR inhibition. Support for our suggested mechanism can be observed in work by Singh et al. who demonstrate that DNA damage activates the H2AFX/H2AX-ATM pathway, followed by AMPK-ULK1 activation and autophagy in epithelial cells.[39] Indeed, after TMZ treatment, DNA damage proteins[31,39] and DNA repair proteins[40,41] may signal the activation of the AMPK-ULK1 axis, which can trigger autophagy both directly through the activation of PIK3C3/VPS34[42] and indirectly by inhibiting MTORC1 through the phosphorylation of raptor.[36] Additionally, we found that the AKT-PI3K pathway becomes chronically suppressed, which can contribute to long-lasting MTOR inhibition and late senescence.[43] Thus, it is plausible to assume that RAPA sensitizes cells to both TMZ-induced autophagy and senescence due to the anticipation of MTOR inhibition, as was observed in skin cancer cells that are exposed to UV radiation[44] and in radiotherapy-treated breast cancer cells.[45] Notwithstanding, RAPA has been shown to modulate senescence, but the role of autophagy in this effect was not determined.[46,47] Therefore, it is not possible to assume that the effect of RAPA is solely through modulation of autophagy.

Malignant gliomas undergo approximately 80% of the oxidative phosphorylation when compared to normal tissues;[48] therefore, a significant reduction in mitochondria through mitophagy could reduce ATP production, despite the proenergetic effects of autophagy. Others have found increases in ATP production after TMZ treatment in glioma,[49] but this has been conducted in a cell line (U251) negative for TP53, whereas U87 is positive for TP53. We hypothesize that TP53

Figure 6 (See previous page). Inhibition of TMZ-induced autophagy triggers apoptosis and reduces senescence in glioma cells. (**A**) *Top*, experimental design. Here, 100 nM bafilomycin A_1 (BafA1) was added on D3 for 24 h, and 2 mM 3-methyladenine (3MA) was added for 1 h on d 3, 4 or 5. *Left graph*, AO graph for BafA1. *Right graph*, AO graph for 3MA. The data are presented as the percentage of AO-positive cells *vs.* AO intensity. (**B**) Representative images of the cells after 3 h, 24 h, and 48 h of 3MA treatment; for the 48 h after 3MA treatment image, 2 representative images are shown to illustrate the apoptotic cells (white arrowhead); ##$P < 0.01$ in relation to TMZ alone on D3; #$P < 0.05$ in relation to TMZ alone on D5 (see **Fig. 2A**); scale bar = 40 μm. (**C**) The Western blot for CASP3. (**D**) The NMA contour plot on D7; NA1, NA2 and NA3 correspond to regions 1, 2, and 3, respectively; SR: small and regular (*i.e.,* apoptotic) nuclei. (**E**) Representative images of the SA-β-gal staining on D7; the numbers denote the percentage of βgal-positive cells; scale bar = 100 μm. #$P < 0.05$ and ##$P < 0.01$ in relation to TMZ alone. (**F**) The percentage of βgal-positive cells. #$P < 0.05$ and ##$P < 0.01$ in relation to TMZ. (**G**) CPD of the cells treated as in (**A**). #$P < 0.05$ in relation to TMZ.

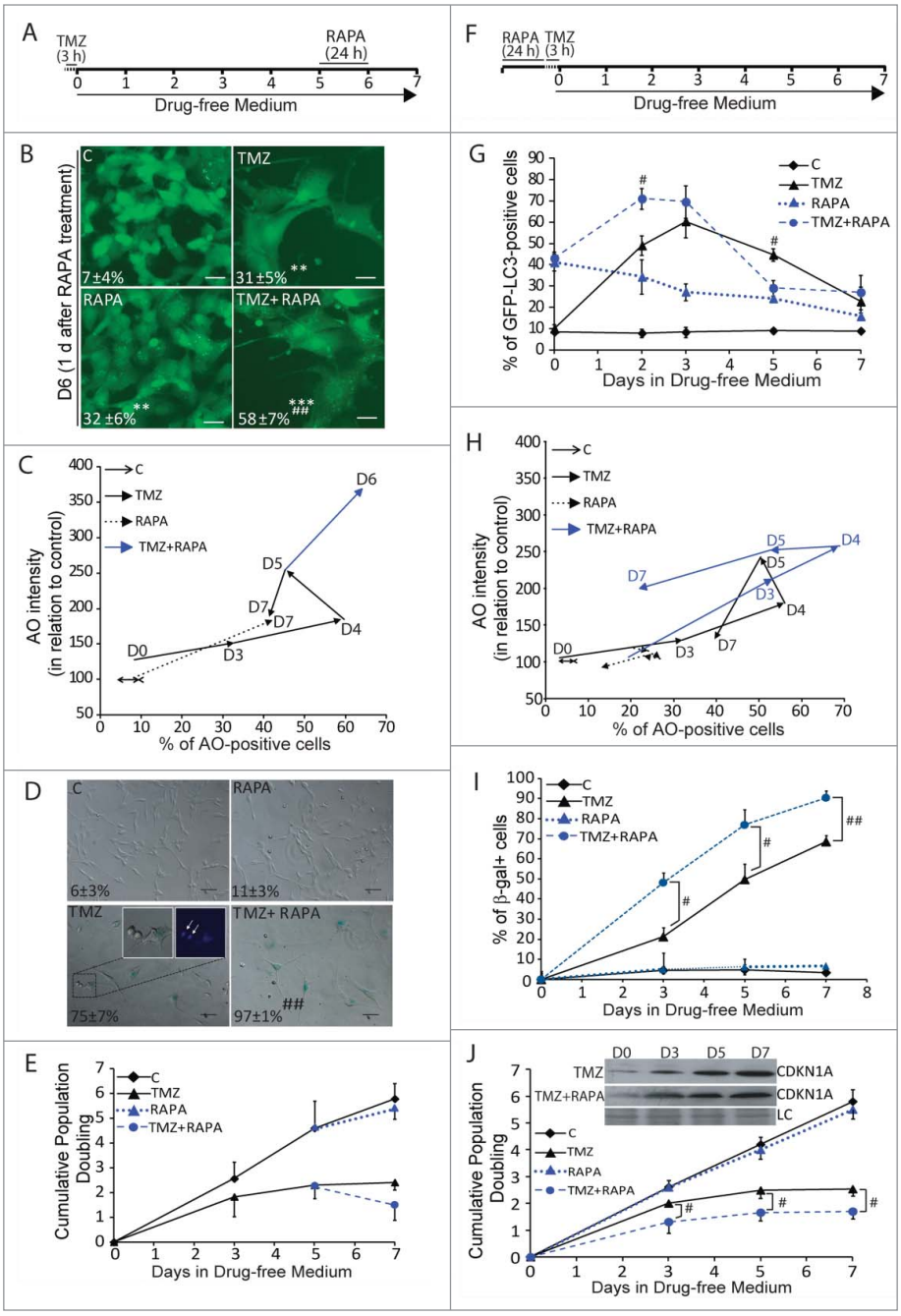

Figure 7. Rapamycin increases TMZ-induced senescence. (**A**) The cells were treated with 100 nM rapamycin (RAPA) on D5 for 24 h. (**B**) Representative images and quantification of GFP-LC3 on D6, 24 h after the RAPA treatment on D5; *$P < 0.05$ and **$P < 0.01$ in relation to the control; ## $P < 0.05$ in relation to TMZ alone. Scale bar = 40 μm. (**C**) AO graphs; the data are presented as the percentage of AO-positive cells *versus* AO intensity. (**D**) SA-β-gal staining on D7 after the treatment as shown in (**A**); detail of the TMZ image pointing to a mitotic figure (white arrow), which was not observed in the TMZ+RAPA treatment; **$P < 0.01$ in relation to TMZ alone; scale bar = 60 μm. (**E**) CPD after treatment as in (**A**). (**F**) The cells were pretreated with 100 nM RAPA 24 h before TMZ. (**G**) The percentage of GFP-LC3-positive cells; #$P < 0.05$ comparing TMZ to TMZ+RAPA. (**H**) AO graphs. (**I**) The percentage of β-gal-positive cells; *$P < 0.05$ and **$P < 0.01$ in relation to TMZ alone. (**J**) CPD and western blot for the CDKN1A/p21 protein after treatment as in (**F**). LC, loading control, *Coomassie blue* stained membrane. #$P < 0.05$ in relation to TMZ alone.

is important in linking DNA damage to mitophagy[41,50] and that in TP53-deficient cells the proenergetic effect of autophagy is not counterbalanced by mitophagy, contrary to the effect in U87. Preliminary data suggest a reduction in total mitochondria after 5 d of the TMZ treatment in U87 cells, supporting this hypothesis.

Population data has shown that the early activation of autophagy, followed by its decrease, is accompanied by a concomitant increase of senescence, in agreement with other models of autophagy and senescence induction.[51,52] In single cells, however, autophagy can decrease before, after or concomitant with cell enlargement. This suggests that autophagy and senescence are not related in a way that the former has to be activated and terminated before the latter can be induced. Additionally, the LC3, nuclear or cellular area status at a given time were not indicative of the previous state or of the outcome regarding autophagy or senescence markers. Because autophagy presents a concerted reduction independent of the cell or nuclear areas on D4, it is plausible to conclude that the kinetics of senescence induction is heterogeneous and unaffected by autophagy kinetics and vice versa. Indeed, autophagy and senescence are triggered in parallel after various stimuli but with different kinetics in the population,[52-54] thus giving the impression of causality that was not observed at the single cell level, as previously hypothesized.[21] Taken together, these data suggest that cells do not need to fully deprive themselves from "autophagocytic" components to then achieve the senescent phenotype and that the machineries responsible for autophagy and senescence can coexist in the cell treated with DNA damage agents.

In support of autophagy not being necessary for senescence induction, senescence occurs at high levels, even after autophagy inhibition in models using RNAi for ATG proteins.[21,53,54] Indeed, the silencing of *Atg5* and *Atg7* only attenuates senescence that is induced by H_2O_2 in fibroblasts [55] and fails to block senescence that is induced by adriamycin in breast

cancer cells,[54] though it highly suppresses autophagy induction. The reduction in the markers of senescence when autophagy is inhibited at the initial and final steps suggests that autophagy may play an important role in supporting the full development of the senescence phenotype, likely by providing ATP to the cell, as indicated in studies with TMZ in gliomas.[49] Additionally, autophagy inhibition reduces the percentage of senescent cells because it targets autophagic cells to undergo apoptosis, as observed in other studies.[39,49]

In several models, autophagy is part of the machinery that generates an adaptive context during cell stress by preventing cells from undergoing apoptosis. In this context, autophagy is permissive for senescence entry, which is the terminal response[56] of those cells that resisted apoptosis.[57] Breast cancer cells exposed to radiation-induced DNA damage trigger autophagy and senescence, and suppression of autophagy increases apoptosis in an amount that is similar to the reduction in senescence. Similar to our results, the combination of radiation+3MA is more cytotoxic than the combination of radiation+BafA1,[58] supporting the proapoptotic effect of early autophagy inhibition with 3MA.

Therefore, the inhibition of autophagy may improve the therapeutic efficiency of DNA damage agents, reducing tumor resistance.[59] Indeed, targeting autophagy in the therapy of aggressive tumors has provided promising results,[15,60] including some clinical trials that have combined classical chemotherapeutics with autophagy activators[61,62] and inhibitors.[63,64] Furthermore, the percentage of cells that remained autophagic on D7 (8%), from which more than 90% were on the NA1 or NA2 area, was closely related to the percentage of cells that retained a clonogenic capacity after the TMZ treatment, as we previously reported.[33]

In fact, the study of different protocols of cancer treatment with autophagy modulation may give important insights regarding the role of autophagy in the long term response of cancer cells to cytotoxic agents, which can predict clinical responses.[65] In this sense, the careful scheduling of chemotherapeutic agents and autophagy modulators may potentiate their effects.

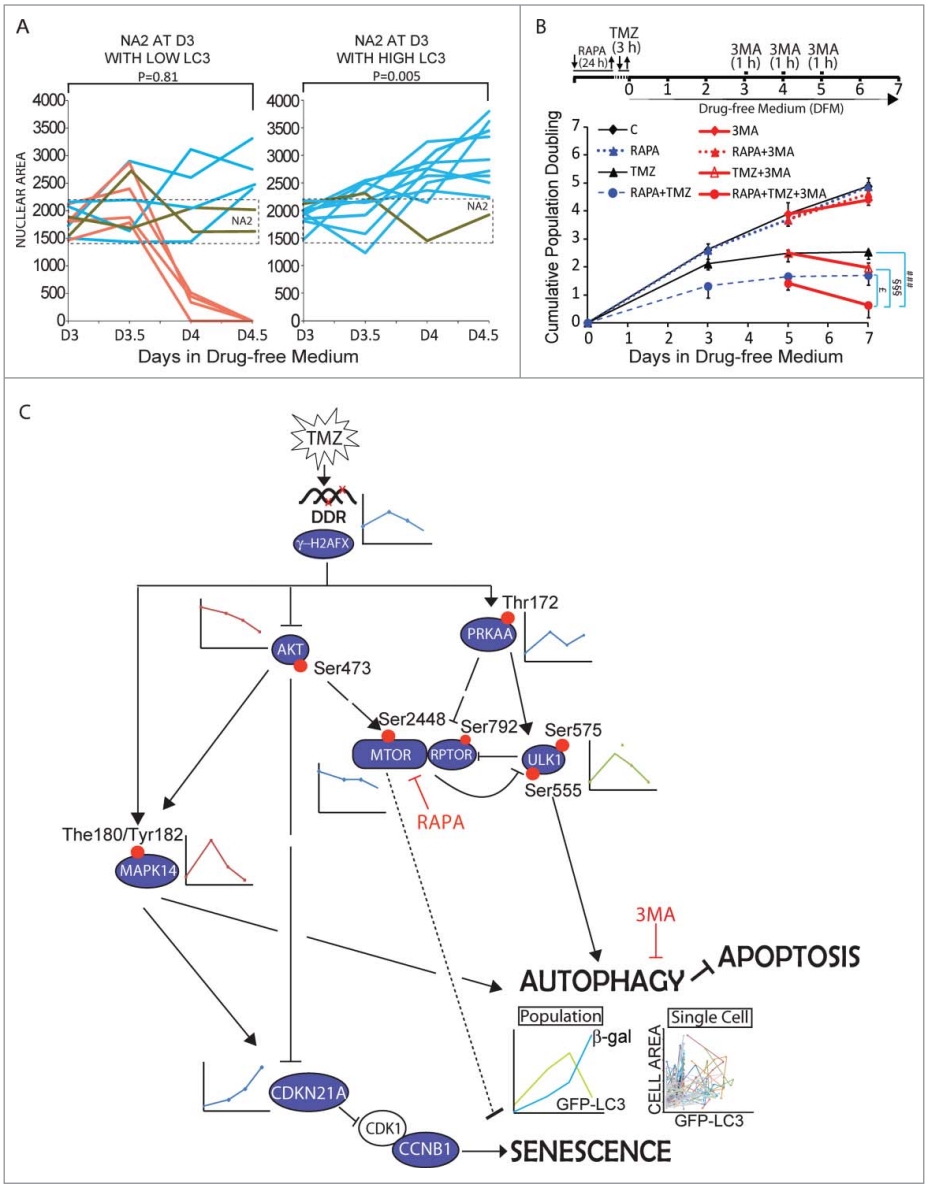

Figure 8. Autophagy activation followed by its inhibition highly increases the toxicity of TMZ *in vitro*. (**A**) Single cell tracks of the nuclear area alterations in the cells with their nuclear areas in the NA2 region separated by both a low (left) and high GFP-LC3 area (right). (**B**) *Top* - the cells were pretreated with 100 nM RAPA for 24 h followed by treatment with 100 mM TMZ for 3 h; 3MA (2 mM) was added for 1 h on d 3, 4, and 5, followed by CPD (*bottom*). ###$P < 0.001$ in relation to TMZ alone, £$P < 0.05$ in relation to TMZ + RAPA and §§§ $P < 0.001$ in relation to TMZ + 3MA. (**C**) Overview of the cellular and molecular effects triggered by TMZ in glioma cells. The sites of phosphorylation are shown as red circles. The dashed line indicates molecular links that may not occur directly or are not yet well established. The broken line from AKT to CDKN1A/p21 indicates a multistep mechanism.

Materials and Methods

Cell culture and treatments

The human GBM cell line U87 stably expressing the autophagic marker GFP-LC3 was kindly provided by Carlos F. M. Menck (University of São Paulo, Brazil). The cells were cultured in low glucose DMEM (11855) that was supplemented with 10% fetal bovine serum (10082147), 1% penicillin/streptomycin and 0.1% amphotericin B at 37°C and 5 % CO_2 in a humidified

incubator; the culture materials (including trypsin, 25200) were obtained from Gibco Laboratories. Temozolomide (T2577), 3-methyladenine (M9281), bafilomycin A_1 (B1793), rapamycin (R0395), and acridine orange (A6014) were purchased from Sigma-Aldrich. The drug vehicle DMSO never exceeded 0.5% (v/v).

Images acquisition and processing

We used a Zeiss Axiovert 200 inverted fluorescence microscope equipped with an Axiocam MRc camera (Carl Zeiss, Jena, Germany). The images were acquired using AxioVision Rel 4.8 Software, at 25°C. Depending on the experiment, the cells were photographed in either low glucose DMEM (single cell experiments and GFP-LC3 images during the experiment) or in 1x phosphate-buffered saline (1x PBS; Gibco, 10010031) (SA-b-gal assay, DAPI and GFP-LC3 at the endpoint of the experiment). The following fluorochromes used were: acridine orange, GFP-LC3 and DAPI. No processing was performed on the images after acquisition.

Cumulative population doubling

For the CPD, the cells were treated with 100 μM TMZ for 3 h, followed by 2 washes and replating of the cells in drug-free medium. After 3, 5, and 7 d in DFM, the cell number was determined, and the CPD was calculated as previously described [66] using the equation $PD = [\log N(t)\text{-}\log N(to)]/\log 2$, where $N(t)$ is the number of cells per well at the time of the count, and $N(to)$ is the initial number of cells. The sum of the PDs was then plotted versus the time of the culture.

GFP-LC3 assay

The U87 cells were transduced using lentivirus with EGFP-LC3, which localizes at the autophagosome after processing.[67] The percentage of cells with at least 5 clear green dots in the cytosol was determined for at least 100 green cells per treatment.[68] We also measured the GFP-LC3 area using Image Pro Plus 6.0 software (Media Cybernetics, Silver Spring, MD, USA). These data were plotted with both the nuclear area and the cell area on a contour plot graph using SigmaPlot software (Systat Software, Inc., San Jose, CA USA).

Acridine orange assay

AO is a marker of acidic vacuolar organelles that fluoresce green in the whole cell but red in acidic compartments (mainly in late autophagosomes/autolysosomes). On the indicated days, the cells were harvested and incubated with 2.7 μM AO for 15 min at room temperature. To quantify the percentage of AO-positive cells and the intensity of the red fluorescence, the AO-stained cells were analyzed in a GUAVA EasyCyte flow cytometer (Guava Technologies, Hayward, CA). The AO data were presented as a plot of the percentage of AO-positive cells *vs.* the red intensity graph to better illustrate the effect of the treatments over time; this plot primarily differentiates between effects that induces the AO-negative cells to become positive (based on a given threshold) from the levels of AO formation.

Western blot

The protein expression and phosphorylation analysis was performed as described,[66,69] with minor modifications. The primary antibodies used were all purchased from Cell Signaling Technology: SQSTM1/p62 (5114), LC3 (12741), pULK1 (S555; 5869), pRPTOR/RPTOR (Ser792) (2083), p-PRKAA/AMPKα (Thr172; 2535), pAKT (Ser473; 4058), p-MTOR (Ser2448; 2971), pRPS6KB1/p70S6K1 (Thr389, Ser371; 9234, 9208), p-EIF4EBP1 (Thr37/Thr46; 2855), pGSK3B (Ser9; 9327), γ-H2AFX/H2AX (Ser139; 9718), pCDC2 (Tyr15; 4539), CCND1/Cyclin D1 (2926), HIST1H3A/C (Ser10; 9701), CDKN1A/p21 (2947), and p-MAPK14/p38 (Thr180/Tyr182; 4511).

Senescence-associated β-galactosidase (SA-β-gal) assay

The cells were treated, washed twice with PBS, and replated at a density of 2×10^4 cells/well in a 12-well plate. At the indicated time, the cells were tested for senescence.[70] Briefly, the cells were washed with ice cold 1x PBS, fixed with 2% paraformaldehyde for 30 min at room temperature and incubated with a fresh SA-β-gal staining solution [1 mg/mL X-gal (Sigma, B4252), 40 mM citric acid/sodium phosphate (pH 6.0), 5 mM potassium ferrocyanide, 5 mM potassium ferricyanide, 150 mM NaCl, and 2 mM $MgCl_2$] for 8 h at 37°C. After, the cell nuclei were stained with 300 nM DAPI for 30 min in the dark. The results are presented as a ratio of the SA-β-gal-positive cells ($\beta\text{-gal}^+$) to the total cells for at least 100 cells per treatment per experiment.

Nuclear morphometric assay (NMA) and contour plot for NMA

The nuclear morphometry was analyzed using a tool developed by our group.[34] Briefly, the cells were treated with TMZ, fixed with 2% paraformaldehyde (v/v in PBS) for 30 min at room temperature and marked with 300 nM DAPI for 30 min at room temperature, followed by quantification of the DAPI-stained nuclei using the Image Pro Plus 6.0 software (Media Cybernetics, Silver Spring, MD, USA) or the ImageJ plugin, which is available at www.ufrgs.br/labsinal/nma. The data are presented as a plot of area versus nuclear irregularity index (NII). Here, we also present a new, alternative presentation of the NMA data depicted as a contour plot graph using SigmaPlot (Systat Software, Inc., San Jose CA, USA).

Cell cycle analysis

For the cell cycle analysis, the cells were treated, followed by 2 washes and replating of the cells in DFM. After 3, 5, and 7 d in DFM, the cells were harvested and fixed in 70% ice-cold ethanol (v/v in PBS) for at least 2 h. The fixed cells were washed with PBS and marked with a solution containing 50 μg/ml propidium iodide (PI), 0.1% Triton X-100 (Life Technologies, HFH-10) and 50 μg/mL RNAse (Life Technologies, 12091–039) for 30 min in the dark at room temperature. The marked cells were analyzed using the flow cytometer GUAVA EasyCyte software to evaluate the DNA content of the cells and the cell cycle distribution of the samples. To separate the singlets from the doublets,

we plotted our data in a graph of red fluor PI (propidium Iodide)-area *per* red fluor (PI)-width. Thus, after a first gate of cells in a graph of forward scatter by side scatter to remove cell debris and cell death, we eliminated the cells with a high PtdIns-width (i.e., the doublets) and only the singlets were evaluated for the cell cycle determination (**Fig. 1C**).

Measurement of ATP intracellular levels

The intracellular ATP levels were measured using the ATP determination kit (Molecular Probes, Invitrogen, A22066). Briefly, the cells were lysed on ice with TE buffer (100 mM Tris, 4 mM EDTA, pH 7.5), and the samples were heated at 95°C for 7 min, followed by centrifugation at 17,200 g for 3 min. The supernatant fraction was used to measure the intracellular ATP levels according to the manufacturer's instructions. The intracellular ATP levels were determined based on an ATP standard curve (1 nM to 1 mM). The total protein amount of the samples was measured with a BCA kit assay to normalize the samples.

Single-cell analysis

For the single-cell analysis, the cells were treated with TMZ 100 μM for 3 h, followed by 2 washes and replating of the cells at a density of 1×10^4 cells per well in a 12-well plate. The same fields were photographed every 12 h, guided by a line on the external surface of the plate. The images obtained were visible with green fluorescence from D3 until D4.5. After, the cell area, the nuclear area and the GFP-LC3 area were determined using Image Pro Plus 6.0 software. For **Fig. 3D**, we separated the intervals of the analysis (i.e., from D3 to 3.5, from D3.5 to 4 and from D4 to 4.5) and converted the initial value of the cell, nuclear and GFP-LC3 areas to 1. Then, we calculated the values of the interval endpoint in relation to 1. For **Fig. 4B and 4C**, we converted the values as relative to D3, which was considered to be 1.

Statistical analysis

The statistical analysis was conducted using TTEST for single comparisons or ANOVA followed by the Student-Newman-Kleus test for multiple comparisons of at least 3 independent experiments; a '*P*' value less than 0.05 was considered significant. A correlation analysis was conducted using the Pearson correlation with Microsoft Excel or PASW Statistics 18.

Disclosure of Potential Conflicts of Interest

No potential conflicts of interest were disclosed.

Acknowledgments

We thank Carlos F Menck and Alexandre T Vessoni for the U87 GFP-LC3 cells, Andrew O. Silva for his insights, Diana Bordin for the reagents and Alexandre T Vessoni, Peter Dunkley, Dirk Van Helden and Charley Staats for critically reading the manuscript. The authors declare no competing financial interests.

Funding

This work was supported by CNPq, 472512/2011-0, ICGEB BRA11/01, Pronex-Fapergs 10/0044-3 and FAPERGS/PRONEN 11/2072-2. ECFC, MMBS, MPT and GL are or were recipients of CNPq fellowships.

Supplemental Material

Supplemental data for this article can be accessed on the publisher's website.

References

1. Parzych KR, Klionsky DJ. An overview of autophagy: morphology, mechanism, and regulation. Antioxid Redox Signal 2014; 20:460-73; PMID:23725295; http://dx.doi.org/10.1089/ars.2013.5371
2. Yang Z, Klionsky DJ. An overview of the molecular mechanism of autophagy. Curr Top Microbiol Immunol 2009; 335:1-32; PMID:19802558
3. Wu WK, Coffelt SB, Cho CH, Wang XJ, Lee CW, Chan FK, Yu J, Sung JJ. The autophagic paradox in cancer therapy. Oncogene 2012; 31:939-53; PMID:21765470; http://dx.doi.org/10.1038/onc.2011.295
4. Minina EA, Sanchez-Vera V, Moschou PN, Suarez MF, Sundberg E, Weih M, Bozhkov PV. Autophagy mediates caloric restriction-induced lifespan extension in Arabidopsis. Aging Cell 2013; 12:327-9; PMID:23331488; http://dx.doi.org/10.1111/acel.12048
5. Pyo JO, Yoo SM, Ahn HH, Nah J, Hong SH, Kam TI, Jung S, Jung YK. Overexpression of Atg5 in mice activates autophagy and extends lifespan. Nat Commun 2013; 4:2300; PMID:23939249; http://dx.doi.org/10.1038/ncomms3300
6. Morselli E, Galluzzi L, Kepp O, Criollo A, Maiuri MC, Tavernarakis N, Madeo F, Kroemer G. Autophagy mediates pharmacological lifespan extension by spermidine and resveratrol. Aging (Albany NY) 2009; 1:961-70; PMID:20157579
7. Toth ML, Sigmond T, Borsos E, Barna J, Erdelyi P, Takacs-Vellai K, Orosz L, Kovács AL, Csikós G, Sass M, et al. Longevity pathways converge on autophagy genes to regulate life span in Caenorhabditis elegans. Autophagy 2008; 4:330-8; PMID:18219227; http://dx.doi.org/10.4161/auto.5618
8. Hansen M, Chandra A, Mitic LL, Onken B, Driscoll M, Kenyon C. A role for autophagy in the extension of lifespan by dietary restriction in C. elegans. PLoS Genet 2008; 4:e24; PMID:18282106; http://dx.doi.org/10.1371/journal.pgen.0040024
9. Takamura A, Komatsu M, Hara T, Sakamoto A, Kishi C, Waguri S, Eishi Y, Hino O, Tanaka K, Mizushima N. Autophagy-deficient mice develop multiple liver tumors. Genes Dev 2011; 25:795-800; PMID:21498569; http://dx.doi.org/10.1101/gad.2016211
10. Inami Y, Waguri S, Sakamoto A, Kouno T, Nakada K, Hino O, Watanabe S, Ando J, Iwadate M, Yamamoto M, et al. Persistent activation of Nrf2 through p62 in hepatocellular carcinoma cells. J Cell Biol 2011; 193:275-84; PMID:21482715; http://dx.doi.org/10.1083/jcb.201102031
11. Duran A, Linares JF, Galvez AS, Wikenheiser K, Flores JM, Diaz-Meco MT, Moscat J. The signaling adaptor p62 is an important NF-kappaB mediator in tumorigenesis. Cancer Cell 2008; 13:343-54; PMID:18394557; http://dx.doi.org/10.1016/j.ccr.2008.02.001
12. Qu X, Yu J, Bhagat G, Furuya N, Hibshoosh H, Troxel A, Rosen J, Eskelinen EL, Mizushima N, Ohsumi Y, et al. Promotion of tumorigenesis by heterozygous disruption of the beclin 1 autophagy gene. J Clin Invest 2003; 112:1809-20; PMID:14638851; http://dx.doi.org/10.1172/JCI20039
13. Xue LY, Chiu SM, Oleinick NL. Atg7 deficiency increases resistance of MCF-7 human breast cancer cells to photodynamic therapy. Autophagy 2010; 6:248-55; PMID:20083906; http://dx.doi.org/10.4161/auto.6.2.11077
14. Maiuri MC, Tasdemir E, Criollo A, Morselli E, Vicencio JM, Carnuccio R, Kroemer G. Control of autophagy by oncogenes and tumor suppressor genes. Cell Death Differ 2009; 16:87-93; PMID:18806760; http://dx.doi.org/10.1038/cdd.2008.131
15. Yang ZJ, Chee CE, Huang S, Sinicrope FA. The role of autophagy in cancer: therapeutic implications. Mol Cancer Ther 2011; 10:1533-41; PMID:21878654; http://dx.doi.org/10.1158/1535-7163.MCT-11-0047
16. Filippi-Chiela EC, Vessoni AT, Menck CF, Lenz G. Autophagy and genomic integrity. Cell Death Differ 2013; PMID:23933813
17. Maes H, Rubio N, Garg AD, Agostinis P. Autophagy: shaping the tumor microenvironment and therapeutic response. Trends Mol Med 2013; 19:428-46; PMID:23714574; http://dx.doi.org/10.1016/j.molmed.2013.04.005

18. Vicencio JM, Galluzzi L, Tajeddine N, Ortiz C, Criollo A, Tasdemir E, Morselli E, Ben Younes A, Maiuri MC, Lavandero S, et al. Senescence, apoptosis or autophagy? When a damaged cell must decide its path-a mini-review. Gerontology 2008; 54:92-9; PMID:18451641; http://dx.doi.org/10.1159/000129697
19. Filippi-Chiela EC, Villodre ES, Zamin LL, Lenz G. Autophagy interplay with apoptosis and cell cycle regulation in the growth inhibiting effect of resveratrol in glioma cells. PLoS One 2011; 6:e20849; PMID:21695150; http://dx.doi.org/10.1371/journal.pone.0020849
20. Marino G, Niso-Santano M, Baehrecke EH, Kroemer G. Self-consumption: the interplay of autophagy and apoptosis. Nat Rev Mol Cell Biol 2014; 15:81-94; PMID:24401948; http://dx.doi.org/10.1038/nrm3735
21. Gewirtz DA. Autophagy and senescence in cancer therapy. J Cell Physiol 2014; 229:6-9; PMID:23794221
22. Gewirtz DA. Autophagy, senescence and tumor dormancy in cancer therapy. Autophagy 2009; 5: 1232-4; PMID:19770583; http://dx.doi.org/10.4161/auto.5.8.9896
23. Rodier F, Campisi J. Four faces of cellular senescence. J Cell Biol 2011; 192:547-56; PMID:21321098; http://dx.doi.org/10.1083/jcb.201009094
24. Collado M, Gil J, Efeyan A, Guerra C, Schuhmacher AJ, Barradas M, Benguría A, Zaballos A, Flores JM, Barbacid M, Beach D, Serrano M, et al. Tumour biology: senescence in premalignant tumours. Nature 2005; 436:642; PMID:16079833; http://dx.doi.org/10.1038/436642a
25. Lenz G. Endogenous Anticancer Mechanisms. Front Biosci 2012; 4:1017-30.
26. Coppe JP, Desprez PY, Krtolica A, Campisi J. The senescence-associated secretory phenotype: the dark side of tumor suppression. Annu Rev Pathol 2010; 5:99-118; PMID:20078217; http://dx.doi.org/10.1146/annurev-pathol-121808-102144
27. Coppe JP, Kauser K, Campisi J, Beausejour CM. Secretion of vascular endothelial growth factor by primary human fibroblasts at senescence. J Biol Chem 2006; 281:29568-74; PMID:16880208; http://dx.doi.org/10.1074/jbc.M603307200
28. Laberge RM, Awad P, Campisi J, Desprez PY. Epithelial-mesenchymal transition induced by senescent fibroblasts. Cancer Microenviron 2012; 5:39-44; PMID:21706180; http://dx.doi.org/10.1007/s12307-011-0069-4
29. Vargas J, Feltes BC, Poloni Jde F, Lenz G, Bonatto D. Senescence; an endogenous anticancer mechanism. Front Biosci (Landmark Ed) 2012; 17:2616-43; PMID:22652801; http://dx.doi.org/10.2741/4074
30. Ben-Porath I, Weinberg RA. The signals and pathways activating cellular senescence. Int J Biochem Cell Biol 2005; 37:961-76; PMID:15743671; http://dx.doi.org/10.1016/j.biocel.2004.10.013
31. Knizhnik AV, Roos WP, Nikolova T, Quiros S, Tomaszowski KH, Christmann M, Kaina B. Survival and death strategies in glioma cells: autophagy, senescence and apoptosis triggered by a single type of temozolomide-induced DNA damage. PLoS One 2013; 8: e55665; PMID:23383259; http://dx.doi.org/10.1371/journal.pone.0055665
32. Kanzawa T, Germano IM, Komata T, Ito H, Kondo Y, Kondo S. Role of autophagy in temozolomide-induced cytotoxicity for malignant glioma cells. Cell Death Differ 2004; 11:448-57; PMID:14713959; http://dx.doi.org/10.1038/sj.cdd.4401359
33. Filippi-Chiela EC, Thome MP, Bueno e Silva MM, Pelegrini AL, Ledur PF, Garicochea B, Zamin LL, Lenz G. Resveratrol abrogates the temozolomide-induced G2 arrest leading to mitotic catastrophe and reinforces the temozolomide-induced senescence in glioma cells. BMC Cancer 2013; 13:147; PMID:23522185; http://dx.doi.org/10.1186/1471-2407-13-147
34. Filippi-Chiela EC, Oliveira MM, Jurkovski B, Callegari-Jacques SM, da Silva VD, Lenz G. Nuclear morphometric analysis (NMA): screening of senescence, apoptosis and nuclear irregularities. PLoS One 2012; 7: e42522; PMID:22905142; http://dx.doi.org/10.1371/journal.pone.0042522
35. Kim J, Kundu M, Viollet B, Guan KL. AMPK and mTOR regulate autophagy through direct phosphorylation of Ulk1. Nat Cell Biol 2011; 13:132-41; PMID:21258367; http://dx.doi.org/10.1038/ncb2152
36. Dunlop EA, Hunt DK, Acosta-Jaquez HA, Fingar DC, Tee AR. ULK1 inhibits mTORC1 signaling, promotes multisite Raptor phosphorylation and hinders substrate binding. Autophagy 2011; 7:737-47; PMID:21460630; http://dx.doi.org/10.4161/auto.7.7.15491
37. Gewirtz DA. Autophagy and senescence: a partnership in search of definition. Autophagy 2013; 9:808-12; PMID:23422284; http://dx.doi.org/10.4161/auto.23922
38. Yamamoto A, Tagawa Y, Yoshimori T, Moriyama Y, Masaki R, Tashiro Y. Bafilomycin A1 prevents maturation of autophagic vacuoles by inhibiting fusion between autophagosomes and lysosomes in rat hepatoma cell line, H-4-II-E cells. Cell Struct Funct 1998; 23:33-42; PMID:9639028; http://dx.doi.org/10.1247/csf.23.33
39. Singh K, Matsuyama S, Drazba JA, Almasan A. Autophagy-dependent senescence in response to DNA damage and chronic apoptotic stress. Autophagy 2012; 8:236-51; PMID:22240589; http://dx.doi.org/10.4161/auto.8.2.18600
40. Zeng X, Kinsella TJ. Mammalian target of rapamycin and S6 kinase 1 positively regulate 6-thioguanine-induced autophagy. Cancer Res 2008; 68:2384-90; PMID:18381446; http://dx.doi.org/10.1158/0008-5472.CAN-07-6163
41. Zeng X, Kinsella TJ. BNIP3 is essential for mediating 6-thioguanine- and 5-fluorouracil-induced autophagy following DNA mismatch repair processing. Cell Res 2010; 20:665-75; PMID:20368736; http://dx.doi.org/10.1038/cr.2010.40
42. Russell RC, Tian Y, Yuan H, Park HW, Chang YY, Kim J, Kim H, Neufeld TP, Dillin A, Guan KL. ULK1 induces autophagy by phosphorylating Beclin-1 and activating VPS34 lipid kinase. Nat Cell Biol 2013; 15:741-50; PMID:23685627; http://dx.doi.org/10.1038/ncb2757
43. Astle MV, Hannan KM, Ng PY, Lee RS, George AJ, Hsu AK, Haupt Y, Hannan RD, Pearson RB. AKT induces senescence in human cells via mTORC1 and p53 in the absence of DNA damage: implications for targeting mTOR during malignancy. Oncogene 2012; 31:1949-62; PMID:21909130; http://dx.doi.org/10.1038/onc.2011.394
44. Strozyk E, Kulms D. The role of AKT/mTOR pathway in stress response to UV-irradiation: implication in skin carcinogenesis by regulation of apoptosis, autophagy and senescence. Int J Mol Sci 2013; 14:15260-85; PMID:23887651; http://dx.doi.org/10.3390/ijms140815260
45. Nam HY, Han MW, Chang HW, Kim SY, Kim SW. Prolonged autophagy by MTOR inhibitor leads radioresistant cancer cells into senescence. Autophagy 2013; 9
46. Pospelova TV, Leontieva OV, Bykova TV, Zubova SG, Pospelov VA, Blagosklonny MV. Suppression of replicative senescence by rapamycin in rodent embryonic cells. Cell Cycle 2012; 11:2402-7; PMID:22672902; http://dx.doi.org/10.4161/cc.20882
47. Demidenko ZN, Zubova SG, Bukreeva EI, Pospelov VA, Pospelova TV, Blagosklonny MV. Rapamycin decelerates cellular senescence. Cell Cycle 2009; 8:1888-95; PMID:19471117; http://dx.doi.org/10.4161/cc.8.12.8606
48. Meixensberger J, Herting B, Roggendorf W, Reichmann H. Metabolic patterns in malignant gliomas. J Neurooncol 1995; 24:153-61; PMID:7562002; http://dx.doi.org/10.1007/BF01078485
49. Katayama M, Kawaguchi T, Berger MS, Pieper RO. DNA damaging agent-induced autophagy produces a cytoprotective adenosine triphosphate surge in malignant glioma cells. Cell Death Differ 2007; 14:548-58; PMID:16946731; http://dx.doi.org/10.1038/sj.cdd.4402030
50. Zeng X, Yan T, Schupp JE, Seo Y, Kinsella TJ. DNA mismatch repair initiates 6-thioguanine-induced autophagy through p53 activation in human tumor cells. Clin Cancer Res 2007; 13:1315-21; PMID:17317843; http://dx.doi.org/10.1158/1078-0432.CCR-06-1517
51. Gamerdinger M, Hajieva P, Kaya AM, Wolfrum U, Hartl FU, Behl C. Protein quality control during aging involves recruitment of the macroautophagy pathway by BAG3. Embo J 2009; 28:889-901; PMID: 19229298; http://dx.doi.org/10.1038/emboj.2009.29
52. Patschan S, Chen J, Polotskaia A, Mendelev N, Cheng J, Patschan D, Goligorsky MS. Lipid mediators of autophagy in stress-induced premature senescence of endothelial cells. Am J Physiol Heart Circ Physiol 2008; 294:H1119-29; PMID:18203850; http://dx.doi.org/10.1152/ajpheart.00713.2007
53. Young AR, Narita M, Ferreira M, Kirschner K, Sadaie M, Darot JF, Tavaré S, Arakawa S, Shimizu S, Watt FM, et al. Autophagy mediates the mitotic senescence transition. Genes Dev 2009; 23:798-803; PMID:19279323; http://dx.doi.org/10.1101/gad.519709
54. Goehe RW, Di X, Sharma K, Bristol ML, Henderson SC, Valerie K, Rodier F, Davalos AR, Gewirtz DA. The autophagy-senescence connection in chemotherapy: must tumor cells (self) eat before they sleep? J Pharmacol Exp Ther 2012; 343:763-78; PMID:22927544; http://dx.doi.org/10.1124/jpet.112.197590
55. Luo Y, Zou P, Zou J, Wang J, Zhou D, Liu L. Autophagy regulates ROS-induced cellular senescence via p21 in a p38 MAPKalpha dependent manner. Exp Gerontol 2011; 46:860-7; PMID:21816217; http://dx.doi.org/10.1016/j.exger.2011.07.005
56. Young AR, Narita M. Connecting autophagy to senescence in pathophysiology. Curr Opin Cell Biol 2010; 22:234-40; PMID:20045302; http://dx.doi.org/10.1016/j.ceb.2009.12.005
57. Collado M, Blasco MA, Serrano M. Cellular senescence in cancer and aging. Cell 2007; 130:223-33; PMID:17662938; http://dx.doi.org/10.1016/j.cell.2007.07.003
58. Huang YH, Yang PM, Chuah QY, Lee YJ, Hsieh YF, Peng CW, Chiu SJ. Autophagy promotes radiation-induced senescence but inhibits bystander effects in human breast cancer cells. Autophagy 2014; 10: 1212-28; PMID:24813621; http://dx.doi.org/10.4161/auto.28772
59. Sui X, Chen R, Wang Z, Huang Z, Kong N, Zhang M, Han W, Lou F, Yang J, Zhang Q, et al. Autophagy and chemotherapy resistance: a promising therapeutic target for cancer treatment. Cell Death Dis 2013; 4:e838; PMID:24113172; http://dx.doi.org/10.1038/cddis.2013.350
60. Kaza N, Kohli L, Roth KA. Autophagy in brain tumors: a new target for therapeutic intervention. Brain Pathol 2012; 22:89-98; PMID:22150924; http://dx.doi.org/10.1111/j.1750-3639.2011.00544.x
61. Reardon DA, Quinn JA, Vredenburgh JJ, Gururangan S, Friedman AH, Desjardins A, Sathornsumetee S, Herndon JE 2nd, Dowell JM, McLendon RE, et al. Phase 1 trial of gefitinib plus sirolimus in adults with recurrent malignant glioma. Clin Cancer Res 2006; 12:860-8; PMID:16467100; http://dx.doi.org/10.1158/1078-0432.CCR-05-2215
62. Chinnaiyan P, Won M, Wen PY, Rojiani AM, Wendland M, Dipetrillo TA, Corn BW, Mehta MP. RTOG 0913: a phase 1 study of daily everolimus (RAD001) in combination with radiation therapy and temozolomide in patients with newly diagnosed glioblastoma. Int J Radiat Oncol Biol Phys 2013; 86:880-4; PMID:23725999; http://dx.doi.org/10.1016/j.ijrobp.2013.04.036

63. Sotelo J, Briceno E, Lopez-Gonzalez MA. Adding chloroquine to conventional treatment for glioblastoma multiforme: a randomized, double-blind, placebo-controlled trial. Ann Intern Med 2006; 144:337-43; PMID:16520474; http://dx.doi.org/10.7326/0003-4819-144-5-200603070-00008
64. Briceno E, Calderon A, Sotelo J. Institutional experience with chloroquine as an adjuvant to the therapy for glioblastoma multiforme. Surg Neurol 2007; 67: 388-91; PMID:17350410; http://dx.doi.org/10.1016/j.surneu.2006.08.080
65. Augustine CK, Yoo JS, Potti A, Yoshimoto Y, Zipfel PA, Friedman HS, Nevins JR, Ali-Osman F, Tyler DS. Genomic and molecular profiling predicts response to temozolomide in melanoma. Clin Cancer Res 2009; 15:502-10; PMID:19147755; http://dx.doi.org/10.1158/1078-0432.CCR-08-1916
66. Zamin LL, Filippi-Chiela EC, Dillenburg-Pilla P, Horn F, Salbego C, Lenz G. Resveratrol and quercetin cooperate to induce senescence-like growth arrest in C6 rat glioma cells. Cancer Sci 2009; 100:1655-62; PMID:19496785
67. Kabeya Y, Mizushima N, Ueno T, Yamamoto A, Kirisako T, Noda T, Kominami E, Ohsumi Y, Yoshimori T. LC3, a mammalian homologue of yeast Apg8p, is localized in autophagosome membranes after processing. Embo J 2000; 19:5720-8; PMID:11060023; http://dx.doi.org/10.1093/emboj/19.21.5720
68. Mizushima N, Yoshimori T, Levine B. Methods in mammalian autophagy research. Cell 2010; 140:313-26; PMID:20144757; http://dx.doi.org/10.1016/j.cell.2010.01.028
69. Zamin LL, Dillenburg-Pilla P, Argenta-Comiran R, Horn AP, Simao F, Nassif M, Gerhardt D, Frozza RL, Salbego C. Protective effect of resveratrol against oxygen-glucose deprivation in organotypic hippocampal slice cultures: Involvement of PI3-K pathway. Neurobiol Dis 2006; 24:170-82; PMID:16860989; http://dx.doi.org/10.1016/j.nbd.2006.06.002
70. Dimri GP, Lee X, Basile G, Acosta M, Scott G, Roskelley C, Medrano EE, Linskens M, Rubelj I, Pereira-Smith O. A biomarker that identifies senescent human cells in culture and in aging skin in vivo. Proc Natl Acad Sci U S A 1995; 92:9363-7; PMID:7568133; http://dx.doi.org/10.1073/pnas.92.20.9363